Featured in Physics

Spontaneous Electrokinetic Magnus Effect

Zachary M. Sherman and James W. Swan*
Department of Chemical Engineering, Massachusetts Institute of Technology, Cambridge, Massachusetts 02139, USA

(Received 31 January 2020; accepted 13 April 2020; published 19 May 2020)

Colloids dispersed in electrolytes and exposed to an electric field produce a locally polarized cloud of ions around them. Above a critical electric field strength, an instability occurs causing these ion clouds to break symmetry leading to spontaneous rotation of particles about an axis orthogonal to the applied field, a phenomenon named Quincke rotation. In this Letter, we characterize a new mode of electrokinetic transport. If the colloids have a net charge, Quincke rotation couples with electrophoretic motion and propels particles in a direction orthogonal to both the applied field and the axis of rotation. This motion is a spontaneous, electrokinetic analogue to the well-known Magnus effect. Typically, motion orthogonal to a field requires anisotropy in particle shape, dielectric properties, or boundary geometry. Here, the electrokinetic Magnus (EKM) effect occurs for spheres with isotropic properties in an unbounded environment, with the Quincke rotation instability providing the broken symmetry needed to drive orthogonal motion. We study the EKM effect using explicit ion, Brownian dynamics simulations and develop a simple, continuum, analytic electrokinetic theory, which are in agreement. We also explain how nonlinearities in the theoretical description of the ions affect Quincke rotation and the EKM effect.

DOI: 10.1103/PhysRevLett.124.208002

A simultaneously translating and rotating object can experience a lift force that propels it orthogonally to its initial direction of motion. This "Magnus effect" is well known for macroscopic objects at large Reynolds numbers [1], but is not typically associated with microscopic objects at small Reynolds numbers. For symmetric objects in isotropic media, like spherical colloids in a Newtonian fluid, linearity of Stokes flow forbids coupled rotation and translation [2]. Khair and Balu reported a Magnus effect for charged spheres of prescribed rotational and translational velocity in an electrolyte due to asymmetry of the local ion cloud [3]. Because there is not a simple way to simultaneously control translation and rotation, field-orthogonal propulsion in electrolytes is usually generated by engineering a break in symmetry [4,5], like synthesizing particles with anisotropic shape [6–9], dielectric properties [10,11], or charge distributions [12] or fabricating walls [13–17] or ratcheted channels [18,19].

In this Letter, we describe a *spontaneous* electrokinetic Magnus (EKM) effect for isotropic, uniformly charged, polarizable colloids in a symmetric, binary electrolyte (Fig. 1, movies S1–S3 in the Supplemental Material [20]). The particles polarize in an electric field $\mathbf{E}_0$ of strength $E_0 \equiv |\mathbf{E}_0|$, producing a locally polarized ion cloud in the direction opposite the field. Above a critical field strength E_c, this orientation becomes unstable, and fluctuations drive the ionic double layer to break symmetry, generating hydrodynamic forces that rotate the colloids about a random axis orthogonal to $\mathbf{E}_0$. This is the well-known phenomenon called Quincke rotation [21]. We have discovered that Quincke rotation couples with electrophoresis to propel a charged particle orthogonally to both the applied field and the axis of rotation, an electrokinetic Magnus effect. The EKM effect occurs for bulk, isotropic particles, with the Quincke rotation instability providing the broken symmetry necessary for orthogonal motion.

Quincke rotation has been well studied in the context of "electrohydrodynamics" (EH), using the Taylor-Melcher leaky dielectric model [22,23], which does not explicitly account for ions, yielding predictions for the critical field E_c and angular velocity Ω [21,24–27],

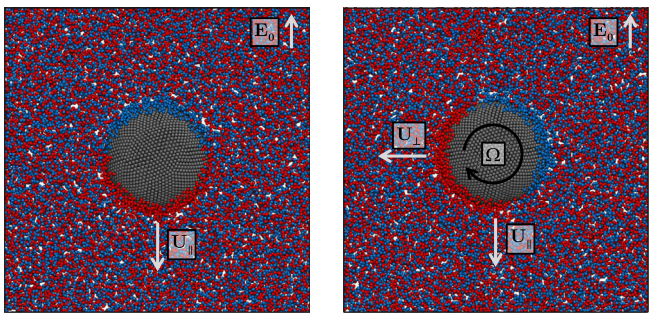

FIG. 1. Left: A negatively charged colloid in an electrolyte with positive (red) and negative (blue) ions polarizes the ion cloud in an electric field $\mathbf{E}_0$ as it moves electrophoretically at velocity $\mathbf{U}_{\|}$. Right: Above E_c, the Quincke rotation instability causes the particle to rotate with angular velocity $\boldsymbol{\Omega}$ about a random axis orthogonal to $\mathbf{E}_0$ and drives the particle orthogonally to both the applied field and axis of rotation with velocity $\mathbf{U}_{\perp}$, the electrokinetic Magnus effect.

$$E_c \equiv \sqrt{\frac{2\eta}{\varepsilon_f \tau_{\mathrm{MW}}(\varepsilon_{pf}-\sigma_{pf})}}, \quad \Omega = \frac{1}{\tau_{\mathrm{MW}}}\sqrt{\left(\frac{E_0}{E_c}\right)^2 - 1}, \qquad (1)$$

where ε_f and ε_p are permittivities of the fluid and particle, σ_f and σ_p are conductivities, $\tau_{\mathrm{MW}} = (\varepsilon_p + 2\varepsilon_f)/(\sigma_p + 2\sigma_f)$, $\varepsilon_{pf} \equiv (\varepsilon_p - \varepsilon_f)/(\varepsilon_p + 2\varepsilon_f)$, and $\sigma_{pf} \equiv (\sigma_p - \sigma_f)/(\sigma_p + 2\sigma_f)$. This scaling of Ω with E_0 has been confirmed in numerous experiments [17,25,27–31]. However, for highly polarizable ($\varepsilon_p \to \infty$) particles, EH predicts $E_c = \Omega = 0$, which is not consistent with our simulations. Because EH approaches contain no information about the ionic double layer, they cannot produce translations driven by electroosmotic flows [23], nor do they offer predictions in terms of experimentally controllable parameters like salt concentration or particle size. In this work, we analyze Quincke rotation and the EKM effect in the context of "electrokinetics" (EK), where the dynamics of ions are explicitly incorporated [32], using both simulation and continuum theory.

Simulation method.—A detailed description is in the Supplemental Material [20]. Here, we offer a brief overview. We carry out Brownian dynamic simulations [33,34] of an ideally polarizable, spherical colloid of radius a and uniform, fixed, surface charge density q_0 in an electrolyte with ions of charge $\pm q_i$ and hydrodynamic radius a_i ($\approx$0.4 nm for simple salts [35]), each at number density n_i, dispersed in a fluid of permittivity ε_f and viscosity η and subject to an electric field $\mathbf{E}_0$. The net charge of the colloid is known, but its induced polarization charge distribution is unknown and varies over time. At each time step, we solve the many-bodied electrostatic problem posed in the Supplemental Material [20] for this charge distribution. The equations of motion for the colloid and ions are integrated in the overdamped limit, taking into account hydrodynamic interactions and Brownian forces [36–41]. Dimensionless variables, indicated by a tilde, are constructed by choosing a_i to be the length scale, the thermal energy k_BT to be the energy scale, the ion diffusion time $\tau_D \equiv 6\pi\eta a_i^3/k_BT$ ($\approx$1 ns) to be the timescale, and $\sqrt{\varepsilon_f a_i k_B T}$ ($\approx 0.2e$) to be the charge scale. This sets the field scale to $\sqrt{k_BT/\varepsilon_f a_i^3}$. We set the total volume fraction of ions to $\phi_i = 0.10$ ($\approx$300 mM) and the ion-ion Coulomb energy at contact to $q_i^2/8\pi\varepsilon_f a_i k_B T = 1$, which yields $\tilde{q}_i \approx 5$ ($\approx 1.60 \times 10^{-19}$ C, i.e., monovalent ions). Counterions were added to balance the net particle charge, and the total number of ions was around 10^5. The electrolyte was equilibrated around the colloid at $E_0 = 0$, and then the field was turned on for up to $200\tau_D$.

Continuum theory and simulation results.—An uncharged, ideally polarizable particle in an electric field $\mathbf{E}_0 \equiv E_0\hat{\mathbf{e}}_z$ instantaneously (compared to τ_D) polarizes with an initial induced surface charge distribution $q_{\mathrm{init}}(\theta,\phi) = 3\varepsilon_f E_0 \cos\theta$ and dipole moment $\mathbf{S}_0 \equiv \int_S dS\mathbf{r}q_{\mathrm{init}} = 4\pi a^3 \varepsilon_f \mathbf{E}_0$, where $\mathbf{r}$ is the position relative to the center, and θ and ϕ are azimuthal and zenith angles. Ions are drawn to opposite induced charges, forming a polarized double layer of thickness $\kappa^{-1} \equiv \sqrt{\varepsilon_f k_B T/2n_i q_i^2}$ (Fig. 1). As ions approach the surface, their electric field induces additional surface charge in the particle, which pulls in more ions, etc., and the particle and double layer "charge up" over time [Fig. 2(a)]. Squires and Bazant [42,43] showed that if $a \gg \kappa^{-1}$, there is an inner region near the surface where ions distribute according to the Poisson-Boltzmann (PB) equation, $-\varepsilon\nabla^2\psi' = \rho$, and an outer region where the electrolyte is charge neutral, $\nabla^2\psi = 0$. $\psi'(\mathbf{r})$ and $\psi(\mathbf{r})$ are the inner and outer potentials and $\rho(\mathbf{r}) = q_i[n_+(\mathbf{r}) - n_-(\mathbf{r})]$ is the charge distribution of the electrolyte in terms of ion concentrations $n_\pm(\mathbf{r})$. If $a \gg \kappa^{-1}$, angular gradients in PB can be neglected, and at a particular θ and ϕ, $\psi'(h)$ is the solution to the one-dimensional PB equation (see Supplemental Material [20]) in a normal coordinate h with a surface charge density $q(\theta,\phi,t)$, the *additional* induced charge excess q_{init}. We assume the inner region equilibrates much faster than the timescale on which q varies, so that ψ'

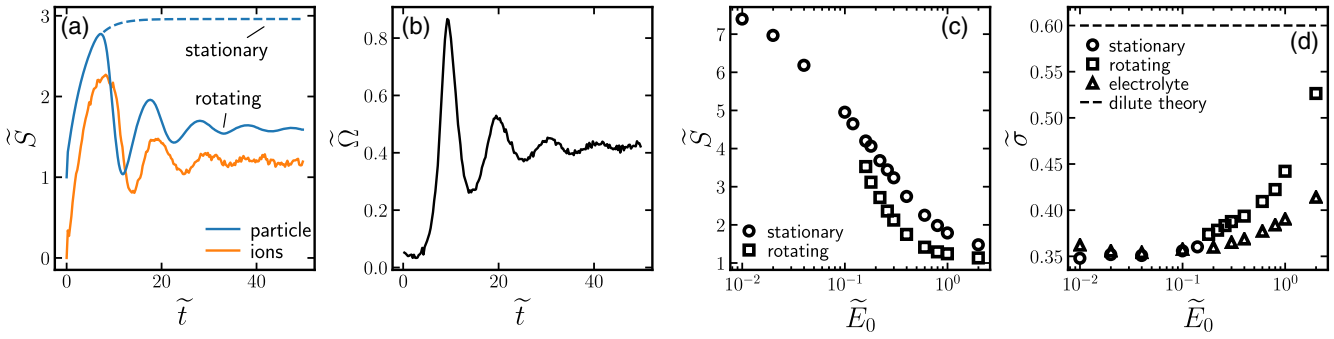

FIG. 2. Particle and ion cloud dipole moments $\tilde{S}$ (a) and angular velocity $\tilde{\Omega}$ (b) over time $\tilde{t}$ from a simulation with $\tilde{a} = 60$ and $\tilde{E}_0 = 0.3$. The steady-state dipole strength (c) and ionic conductivity $\tilde{\sigma}$ (d) for rotating particles, nonrotating particles, and pure electrolyte for $\tilde{a} = 30$. For $E_0 > E_c$, the "stationary" dipole in (c) was extracted from an exponential fit to the stationary regime, like the dashed line in (a). In (d), $\sigma = n_i q_i^2/3\pi\eta a_i$ is the dilute theoretical value [42].

satisfies PB in a pseudosteady sense. Angular and time dependence of ψ' come solely from the boundary condition $q(\theta,\phi,t)$.

The inner potential as $h \to \infty$, denoted $\psi'_p - \zeta$, where ψ'_p is the particle surface potential and ζ is the potential drop across the double layer (i.e., the zeta potential), must equal the outer potential ψ at the surface. Because the particle is ideally polarizable with $\psi'_p = 0$, $\psi(r=a,\theta,\phi,t) = -\zeta(\theta,\phi,t)$. Therefore, ψ in the neutral region of the electrolyte can be expressed as

$$\psi(\mathbf{r},t) = -\mathbf{E}_0 \cdot \mathbf{r}\left(1 - \frac{a^3}{r^3}\right) + \sum_{\ell m} \frac{C_{\ell m}(t)}{r^{\ell+1}} Y_{\ell m}(\theta,\phi), \quad (2)$$

where $C_{\ell m}(t) = -a^{\ell+1}\int_\Gamma d\Gamma \zeta(\theta,\phi,t) Y_{\ell m}(\theta,\phi)$, $Y_{\ell m}$ is the spherical harmonic of degree ℓ and order m, and Γ is the unit sphere. ψ satisfies the initial conditions with $\zeta(\theta,\phi,0) = C_{\ell m}(0) = 0$. In the bulk electrolyte, there is a local current density $\mathbf{j}(\mathbf{r},t) = \sigma \mathbf{E}(\mathbf{r},t)$ due to mobile ions, where $\mathbf{E} \equiv -\nabla\psi$ and σ is the electrolyte conductivity. The current entering the double layer, $-\mathbf{j}(a,\theta,\phi,t)\cdot\hat{\mathbf{r}}$, induces equal and opposite surface charges $q(\theta,\phi,t)$ in the particle to satisfy inner region electroneutrality. If the particle also rotates with angular velocity $\mathbf{\Omega}$, we can construct a conservation equation for the induced charge

$$\frac{\partial q(\theta,\phi,t)}{\partial t} = \sigma \mathbf{E}\cdot\hat{\mathbf{r}} - \nabla_s \cdot q\mathbf{\Omega}\times\mathbf{r}, \quad (3)$$

where ∇_s is the surface gradient. The particle is torque-free, so $\mathbf{\Omega}$ is set by the balance of the electric torque driving rotation, $\mathbf{S}_i \times \mathbf{E}_0 = -\int_S dS \mathbf{r} q \times \mathbf{E}_0$, where $\mathbf{S}_i$ is the net dipole of the ion cloud, and the opposing hydrodynamic torque, $-8\pi\eta a^3 \mathbf{\Omega}$, yielding $\mathbf{\Omega} = -\int_S dS \mathbf{r} q \times \mathbf{E}_0 / 8\pi\eta a^3$ [2,26,44]. The induced charge and zeta potential are related through PB, admitting a charge-voltage relation $q(\zeta)$ and differential capacitance $C(\zeta) \equiv dq/d\zeta$, and Eq. (3) can be written solely in terms of ζ,

$$C(\zeta)\frac{\partial\zeta}{\partial t} = \sigma\mathbf{E}\cdot\hat{\mathbf{r}} + \frac{\nabla_s \cdot q(\zeta)}{8\pi\eta a^3}\left(\int_S dS \mathbf{r} q(\zeta) \times \mathbf{E}_0\right)\times\mathbf{r}. \quad (4)$$

We choose coordinates where $\mathbf{E}_0 = E_0\hat{\mathbf{e}}_z$ and $\mathbf{\Omega} = \Omega\hat{\mathbf{e}}_y$ and convert Eq. (4) into an equation involving only the $C_{\ell m}$ coefficients by multiplying by $Y_{\ell m}$ and integrating over Γ. For $\zeta q_i / k_B T \ll 1$, we use the Debye-Huckel (DH) solution to the PB equation with a Stern layer of thickness a_i to account for the ions' finite distance of closest approach,

$$q = \varepsilon_f \kappa \zeta/(1+\kappa a_i), \qquad C = \varepsilon_f \kappa/(1+\kappa a_i). \quad (5)$$

Setting $a_i = 0$ recovers the original DH solution. $C_{\ell m}(t) = 0$ for $\ell \geq 2$, and the three equations for $\ell = 1$ admit three steady-state solutions where $\partial C_{\ell m}/\partial t = 0$, with angular velocities

$$\Omega = 0, \pm\frac{1}{\tau_c}\sqrt{\left(\frac{E_0}{E_c}\right)^2 - 1}, \quad E_c \equiv \sqrt{\frac{8\eta\sigma(1+\kappa a_i)^2}{\varepsilon_f^2 \kappa^2 a^2}}, \quad (6)$$

where $\tau_c \equiv \varepsilon_f \kappa a / 2\sigma(1+\kappa a_i)$ is the charging timescale [42,43].

A detailed derivation of Eq. (6) is in the Supplemental Material [20]. The $\Omega \neq 0$ solutions are only real above a critical field strength E_c. A linear stability analysis (see Supplemental Material [20]) reveals that the stationary ($\Omega = 0$) solution is stable below E_c and unstable above E_c, while the rotating solutions are stable for $E_0 > E_c$. These EK expressions (6) are similar to the EH expressions (1) but in terms of experimentally controllable parameters, with τ_c replacing τ_{MW} and dependence on κa. In particular, E_c decreases with particle size as $E_c \sim a^{-1}$, unlike Eq. (1) which is independent of a. For large fields, Eq. (6) becomes $\Omega \approx E_0\sqrt{\sigma/2\eta}$ and is independent of a, consistent with EH predictions. Equation (6) also shares features with EH expressions for Quincke rotation of dielectric shells and vesicles [45–48], where here the double layer acts as a thin dielectric capacitor. For typical values in water at 10 mM ionic strength, E_c can be written as a voltage drop across the particle, $E_c \approx 0.09\ \mathrm{V}/a$, i.e., a 1 μm particle has $E_c \approx 900$ V/cm. Though such large field strengths might be difficult to achieve experimentally in aqueous electrolytes, larger particles have lower E_c (a 10 μm particle has $E_c \approx 90$ V/cm), a more electrochemically stable organic-based electrolyte can be chosen, or alternating current (ac) fields can be used. The stable, steady-state particle dipole is

$$\tilde{\mathbf{S}} = \begin{cases} \left(1 + \frac{\kappa a}{2(1+\kappa a_i)}\right)\hat{\mathbf{e}}_z, & E_0 \leq E_c \\ \pm\frac{\kappa a}{2(1+\kappa a_i)}\frac{E_c}{E_0}\sqrt{1 - \left(\frac{E_c}{E_0}\right)^2}\hat{\mathbf{e}}_x & \\ \quad + \left(1 + \frac{\kappa a}{2(1+\kappa a_i)}\left(\frac{E_c}{E_0}\right)^2\right)\hat{\mathbf{e}}_z, & E_0 > E_c \end{cases}, \quad (7)$$

where $\tilde{\mathbf{S}} \equiv \mathbf{S}/S_0$. Figures 2(a)–2(b) show the charging and rotation dynamics in simulations, while Figs. 3(a)–3(b) compare steady-state values between simulations and theory. Below E_c, the particle dipole is aligned with $\mathbf{E}_0$ and charges monotonically over τ_c to a value independent of E_0. Above E_c, the particle is initially nonrotating, but eventually ions accumulated at the poles become unstable and spill over the sides of the particle. The ions' hydrodynamic interactions with the surface rotate the particle. The dipole strength $\tilde{S} \equiv |\tilde{\mathbf{S}}|$ drops [Fig. 2(c)] and breaks symmetry to point off-axis relative to $\mathbf{E}_0$. $\tilde{S}$ decreases with $\tilde{E}_0$ as charge is convected away, and $\tilde{S} \to 1$ at large $\tilde{E}_0$. Our theory underpredicts E_c and overpredicts Ω from simulations, which also occurs with experiments [30,31], but overall agrees. Because rotation facilitates ion convection, it increases the electrolyte's conductivity σ compared to pure electrolyte [Fig. 2(d)], increasing with E_0 as Ω

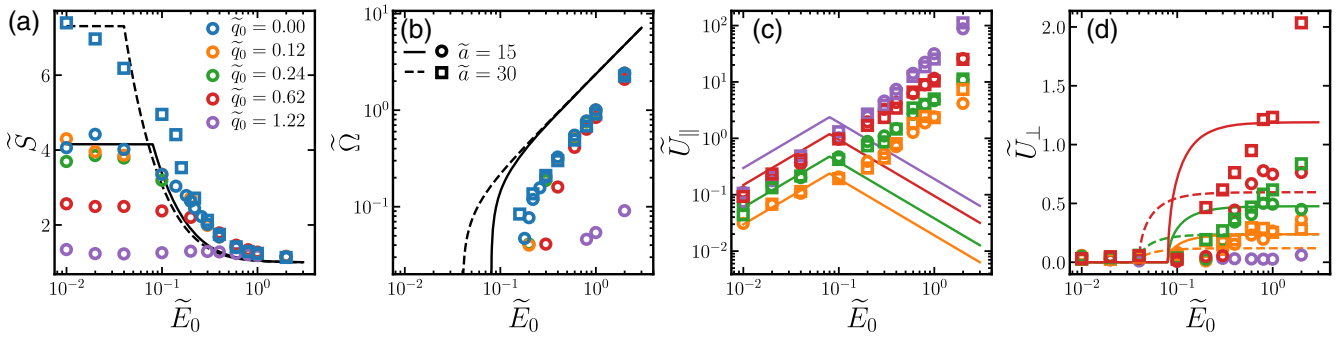

FIG. 3. The dipole strength $\tilde{S}$ (a), angular velocity $\tilde{\Omega}$ (b), electrophoretic velocity $\tilde{U}_\parallel$ (c), and Magnus velocity $\tilde{U}_\perp$ (d) for different particle sizes $\tilde{a}$ (different shapes and line styles) and net charges $\tilde{q}_0$ (different colors) as a function of external field $\tilde{E}_0$ from simulation (symbols) and theory (lines).

increases. This conductivity increase above E_c due to Quincke rotation has also been measured in experiments [49]. The response of the ion cloud lags that of the particle, leading to coupled oscillations in S and Ω [Fig. 2(a)]. The ions can be imagined as imparting "inertia" to the colloid dipole, and the dynamics become chaotic at very large fields [25,31].

The induced $q_{\text{init}} + q$ contributes no net charge to the particle. If the particle has a net charge, it is due to fixed charges $q_0 = \varepsilon_f \kappa \zeta_0/(1+\kappa a_i)$, where ζ_0 is the net zeta potential. Because PB is linear with the DH approximation, $\zeta(\theta,\phi,t)$ for a neutral particle can be superimposed with ζ_0. The fluid velocity at the particle surface is $\mathbf{u} = -\varepsilon_f(\zeta_{0,D}+\zeta_D)\mathbf{E}_t/\eta$, where $\zeta_{0,D} = q_0/\varepsilon_f\kappa$ and $\zeta_D = q/\varepsilon_f\kappa$ are voltage drops across the diffuse region of the double layer and $\mathbf{E}_t$ is the field tangent to the surface [42]. The particle's translational velocity is obtained by integrating $\mathbf{u}$ over its surface, $\mathbf{U} = -\int_S dS\mathbf{u}/4\pi a^2$ [50],

$$\mathbf{U} = \begin{cases} \frac{\varepsilon_f \zeta_{0,D} E_0}{\eta}\hat{\mathbf{e}}_z & E_0 \le E_c \\ \frac{\varepsilon_f \zeta_{0,D} E_c}{\eta}\left(\pm\sqrt{1-(\frac{E_c}{E_0})^2}\hat{\mathbf{e}}_x + \frac{E_c}{E_0}\hat{\mathbf{e}}_z\right) & E_0 > E_c \end{cases}, \tag{8}$$

Below E_c, the particle moves electrophoretically with a well-known expression in the thin double layer limit [51] that is independent of a and agrees with our simulations [Fig. 3(c)]. Above E_c while rotating, the velocity has a component orthogonal to the field, i.e., the EKM effect. The Magnus velocity, $U_\perp \equiv \mathbf{U}\cdot\hat{\mathbf{e}}_x$, increases with E_0, saturating at a value $U_{\perp,\max} \equiv \varepsilon_f\zeta_{0,D}E_c/\eta$ that agrees with our simulations for small $\tilde{q}_0$ [Fig. 3(d)]. For a 1 μm particle with $\zeta_{0,D} \approx 50$ mV, $U_\perp \approx 3$ mm/s, which is fast compared to diffusion, $k_BT/6\pi\eta a^2 \approx 1$ μm/s. Equation (8) predicts $U_{\perp,\max} \sim E_c \sim a^{-1}$, while our simulations show that $U_{\perp,\max}$ generally increases with a. Our theory predicts that the electrophoretic velocity, $U_\parallel \equiv \mathbf{U}\cdot\hat{\mathbf{e}}_z$, decreases with increasing $E_0 > E_c$ as the ion cloud dipole aligns orthogonally to $\mathbf{E}_0$ and $\mathbf{E}_t$ becomes symmetric about $\hat{\mathbf{e}}_x$, prohibiting translation in the $\hat{\mathbf{e}}_z$ direction. However, we observe a linear increase in $U_\parallel$ with E_0, and the classical electrophoresis formula for $E_0 \le E_c$ seems to hold for simulations above E_c while the particle rotates.

Nonlinear effects.—The charge conservation equation (3) neglects surface conduction, angular diffusion, and translational convection, which become important at large $\tilde{E}_0$ [42,52]. The analysis assumes a thin double layer and uses

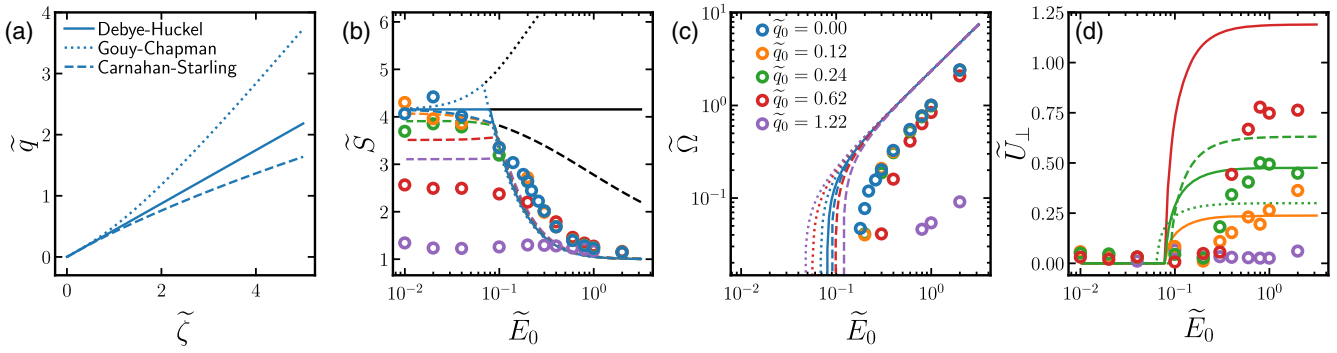

FIG. 4. (a) Surface charge density $\tilde{q}$ as a function of zeta potential $\tilde{\zeta}$ for various ion models, accounting for Stern layers. Simulation (symbols) and theoretical results (lines) for the dipole strength $\tilde{S}$ (b), angular velocity $\tilde{\Omega}$ (c), and Magnus velocity $\tilde{U}_\perp$ as a function of external field $\tilde{E}_0$ for $\tilde{a} = 15$. In (b), the unstable stationary solutions above E_c are shown in black.

the Debye-Huckel approximation, which is inaccurate at large ionic strength and ζ. Finally, fluctuations of the particle, surface charge, and ion cloud are not incorporated. Despite these shortcomings, there is fair agreement with our simulations where these complicated effects are accounted for. To address some of these issues, nonlinearities in the description of the ions can be incorporated into the Poisson-Boltzmann equation, which modify $q(\zeta)$ and $C(\zeta)$ [Fig. 4(a)]. In addition to the linear Debye-Huckel (DH) solution, we consider the Gouy-Chapman (GC) model, in which ions do not interact but obey the nonlinear PB equation, and the Carnahan-Starling (CS) model that accounts for steric repulsions among ions [35]. Details are discussed in the Supplemental Material [20]. Because the Gouy-Chapman capacitance $C(\zeta)$ increases with ζ, the particle dipole increases with E_0 in the stationary regime [Fig. 4(b)]. On the other hand, the Carnahan-Starling capacitance decreases with ζ, so $\tilde{S}$ decreases with E_0. The rotational instability is driven by the dipole strength, so GC has a lower E_c than DH, while CS has a larger E_c than DH [Fig. 4(c)]. Above E_c, the induced ζ generally decreases with E_0, so both the GC and CS solutions approach the DH solution at large E_0. If the particle has a net charge, the double layer screens both q and q_0. For linear DH, these situations can be superimposed, and q_0 does not affect charging or Quincke rotation. This superposition fails for nonlinear models, and $q(\zeta)$ and $C(\zeta)$ must be replaced with $q(\zeta_0+\zeta)$ and $C(\zeta_0+\zeta)$ in Eq. (4). For small $\tilde{q}_0$ with $\zeta_0 \ll \zeta$, this contributes negligibly to the theory and simulations. As $\tilde{q}_0$ increases and $\zeta_0 \gtrsim \zeta$, the net charge hinders charging and rotation, suppressing them altogether for large $\tilde{q}_0$ in the simulations [Figs. 4(b)–4(c)]. In the theory, the charged GC solutions begin with a larger $C(\zeta_0) > C(0)$ and have larger $\tilde{S}$ and smaller E_c than the uncharged case, opposite the trends observed in the simulations. The charged CS solutions begin with a smaller $C(\zeta_0) < C(0)$ and have smaller $\tilde{S}$ and larger E_c than the uncharged case, consistent with, but less pronounced than, simulation results. At large E_0, solutions collapse to the DH values, so q_0 does not affect $\tilde{S}$ or $\tilde{\Omega}$. However, the Magnus velocity is still sensitive to the ion model through $\zeta_{0,D}$ [Fig. 4(d)]. For a given q_0, the GC $\zeta_{0,D}$ and E_c are smaller than the DH $\zeta_{0,D}$ and E_c, so $U_{\perp,\max}$ is smaller. Similarly, the CS $\zeta_{0,D}$ and E_c are larger than the DH values, so $U_{\perp,\max}$ is larger.

Conclusion.—We reported a spontaneous electrokinetic Magnus effect for polarizable colloids in an electrolyte. We used electrokinetic methods to investigate the phenomenon, including explicit ion Brownian dynamics simulations and analytic results from a continuum theory, overcoming shortcomings of electrohydrodynamic methods. The analytic expressions offer useful scaling predictions to guide experiments, while the simulations provide a high-fidelity model of the complicated physics involved. We envision applications for the EKM effect in self-propelling active matter, which typically involves complicated particle designs [53–56] or living organisms [57,58]. Because the Magnus velocity is decoupled from the field, it offers a tunable self-propulsion mechanism using simple materials. Quincke rotors are already used in active matter but require boundaries [15,16] or anisotropic particles [9] whereas the EKM effect occurs for spheres in unbounded domains. Other applications include controlling electrorheological responses with rotating particles [30,59,60] and leveraging the Magnus velocity for particle separation.

We thank Martin Z. Bazant for helpful discussion. We thank support from NASA (Grant No. 80NSSC18K0162) and NSF (Career Grant No. 1554398).

*jswan@mit.edu

[1] L. Briggs, Am. J. Phys. **27**, 589 (1959).
[2] S. Kim and S. J. Karrila, *Microhydrodynamics: Principles and Selected Applications* (Dover Publications, Mineola, 2005).
[3] A. Khair and B. Balu, Electrophoresis **40**, 2407 (2019).
[4] D. Long and A. Ajdari, Phys. Rev. Lett. **81**, 1529 (1998).
[5] T. M. Squires and M. Z. Bazant, J. Fluid Mech. **560**, 65 (2006).
[6] E. Yariv, Phys. Fluids **17**, 051702 (2005).
[7] F. Ma, S. Wang, D. T. Wu, and N. Wu, Proc. Natl. Acad. Sci. U.S.A. **112**, 6307 (2015).
[8] A. M. Brooks, S. Sabrina, and K. J. M. Bishop, Proc. Natl. Acad. Sci. U.S.A. **115**, E1090 (2018).
[9] D. Das and E. Lauga, Phys. Rev. Lett. **122**, 194503 (2019).
[10] S. Gangwal, O. J. Cayre, M. Z. Bazant, and O. D. Velev, Phys. Rev. Lett. **100**, 058302 (2008).
[11] J. G. Lee, A. M. Brooks, W. A. Shelton, K. J. M. Bishop, and B. Bharti, Nat. Commun. **10**, 2575 (2019).
[12] A. J. Mowitz and T. A. Witten, Phys. Rev. E **96**, 062613 (2017).
[13] E. Yariv, Phys. Fluids **18**, 031702 (2006).
[14] M. S. Kilic and M. Z. Bazant, Electrophoresis **32**, 614 (2011).
[15] A. Bricard, J.-B. Caussin, N. Desreumaux, O. Dauchot, and D. Bartolo, Nature (London) **503**, 95 (2013).
[16] A. Bricard, J.-B. Caussin, D. Das, C. Savoie, V. Chikkadi, K. Shitara, O. Chepizhko, F. Peruani, D. Saintillan, and D. Bartolo, Nat. Commun. **6**, 7470 (2015).
[17] G. E. Pradillo, H. Karani, and P. M. Vlahovska, Soft Matter **15**, 6564 (2019).
[18] A. M. Drews, H.-Y. Lee, and K. J. M. Bishop, Lab Chip **13**, 4295 (2013).
[19] K. J. M. Bishop, A. M. Drews, C. A. Cartier, S. Pandey, and Y. Dou, Langmuir **34**, 6315 (2018).
[20] See Supplemental Material at http://link.aps.org/supplemental/10.1103/PhysRevLett.124.208002 for simulation movies and additional details of the simulation method and continuum theory.
[21] T. B. Jones, IEEE Trans. Ind. Appl. **IA-20**, 845 (1984).
[22] J. R. Melcher and G. I. Taylor, Annu. Rev. Fluid Mech. **1**, 111 (1969).
[23] D. A. Saville, Annu. Rev. Fluid Mech. **29**, 27 (1997).

[24] I. Turcu, J. Phys. A **20**, 3301 (1987).
[25] E. Lemaire and L. Lobry, Physica (Amsterdam) **314A**, 663 (2002).
[26] D. Das and D. Saintillan, Phys. Rev. E **87**, 043014 (2013).
[27] P. M. Vlahovska, Annu. Rev. Fluid Mech. **51**, 305 (2019).
[28] P. E. Secker and I. N. Scialom, J. Appl. Phys. **39**, 2957 (1968).
[29] T. Coddington, A. F. Pollard, and H. House, J. Phys. D **3**, 1212 (1970).
[30] L. Lobry and E. Lemaire, J. Electrost. **47**, 61 (1999).
[31] F. Peters, L. Lobry, and E. Lemaire, Chaos **15**, 013102 (2005).
[32] M. Z. Bazant, J. Fluid Mech. **782**, 1 (2015).
[33] J. A. Anderson, C. D. Lorenz, and A. Travessat, J. Comput. Phys. **227**, 5342 (2008).
[34] J. Glaser, T. D. Nguyen, J. A. Anderson, P. Lui, F. Spiga, J. A. Millan, D. C. Morse, and S. C. Glotzer, Comput. Phys. Commun. **192**, 97 (2015).
[35] M. Z. Bazant, M. S. Kilic, B. D. Storey, and A. Ajdari, Adv. Colloid Interface Sci. **152**, 48 (2009).
[36] J. W. Swan and G. Wang, Phys. Fluids **28**, 011902 (2016).
[37] A. M. Fiore, F. B. Usabiaga, A. Donev, and J. W. Swan, J. Chem. Phys. **146**, 124116 (2017).
[38] A. Fiore and J. Swan, J. Chem. Phys. **148**, 044114 (2018).
[39] D. M. Heyes and J. R. Melrose, J. Non-Newtonian Fluid Mech. **46**, 1 (1993).
[40] Z. Varga, G. Wang, and J. Swan, Soft Matter **11**, 9009 (2015).
[41] G. Wang, A. M. Fiore, and J. W. Swan, J. Rheol. **63**, 229 (2019).
[42] T. M. Squires and M. Z. Bazant, J. Fluid Mech. **509**, 217 (2004).
[43] M. Z. Bazant and T. M. Squires, Phys. Rev. Lett. **92**, 066101 (2004).
[44] J. D. Jackson, *Classical Electrodynamics* (John Wiley & Sons, Hoboken, 1998).
[45] T. B. Jones, *Electromechanics of Particles* (Cambridge University Press, Cambridge, England, 1995).
[46] I. Turcu and C. M. Lucaciu, J. Phys. A **22**, 985 (1989).
[47] I. Turcu and C. M. Lucaciu, J. Phys. A **22**, 995 (1989).
[48] P. F. Salipante, R. L. Knorr, R. Dimova, and P. M. Vlahovska, Soft Matter **8**, 3810 (2012).
[49] N. Pannacci, L. Lobry, and E. Lemaire, Phys. Rev. Lett. **99**, 094503 (2007).
[50] H. A. Stone and A. D. T. Samuel, Phys. Rev. Lett. **77**, 4102 (1996).
[51] W. B. Russel, D. A. Saville, and W. R. Schowalter, *Colloidal Dispersions* (Cambridge University Press, Cambridge, England, 1989).
[52] F. Peters, l. Lobry, A. Khayari, and E. Lemaire, J. Chem. Phys. **130**, 194905 (2009).
[53] W. F. Paxton, K. C. Kistler, C. C. Olmeda, A. Sen, S. K. St. Angelo, Y. Cao, T. E. Mallouk, P. E. Lammert, and V. H. Crespi, J. Am. Chem. Soc. **126**, 13424 (2004).
[54] T. Sanchez, D. T. N. Chen, S. J. DeCamp, M. Heymann, and Z. Dogic, Nature (London) **491**, 431 (2012).
[55] C. W. Shields IV, K. Han, F. Ma, T. Miloh, G. Yossifon, and O. D. Velev, Adv. Funct. Mater. **28**, 1803465 (2018).
[56] A. M. Brooks, M. Tasinkevych, S. Sabrina, D. Velegol, A. Sen, and K. J. M. Bishop, Nat. Commun. **10**, 495 (2019).
[57] R. Di Leonardo, L. Angelani, D. Dell'Arciprete, G. Ruocco, V. Iebba, S. Schippa, M. P. Conte, F. Mecarini, F. De Angelis, and E. Di Fabrizio, Proc. Natl. Acad. Sci. U.S.A. **107**, 9541 (2010).
[58] E. Lauga, Annu. Rev. Fluid Mech. **48**, 105 (2016).
[59] N. Pannacci, E. Lemaire, and L. Lobry, Rheol. Acta **46**, 899 (2007).
[60] E. Lemaire, L. Lobry, N. Pannacci, and F. Peters, J. Rheol. **52**, 769 (2008).